Study of the Propagation Characteristics of Chirped Pierce-Gaussian Beams in both Free Space and PT-Symmetric Media

Zhengchun Zhao, Bing Wen*, Yangbao Deng*, Chunhui Gao, Lixiong Li, Sheng Li

***Abstract*—This paper investigates the propagation characteristics of chirped Pierce-Gaussian beams in both free space and PT-symmetric media using the stepwise Fourier method. An in-depth analysis is conducted on the effects of the truncation factor, chirp factor, modulation depth, and gain/loss coefficient of the medium. When the wave propagates in free space, the truncation factor modulates its focusing intensity, and the initial chirp controls the direction of beam deflection. Conversely, when propagated via a PT-symmetric medium, the Pierce-Gaussian beam emits a soliton at the focal point and attains reliable propagation. The modulation strength P and gain/loss coefficient W_0 of the PT-symmetric medium impact the shedding soliton's peak intensity and oscillation period. Meanwhile, the beam's initial chirp parameter c can regulate the peak intensity of the shedding soliton. The results of this study offer a significant theoretical foundation for understanding the dynamics of the propagation of specialized beams.**

***Index Terms*—chirp; Pierce-Gaussian; free space; PT-symmetric; propagation**

I. Introduction

The Pearcey function was initially presented in 1946 by T. Pearcey as part of his investigation into the computation of diffraction integrals for pointed focal dispersion [1]. In 2012, Ring et al. introduced the concept of the Pierce beam, which is associated with the Pierce function [2]. Pierce beam has characteristics such as a simple functional structure, self-repairing, self-focusing, maintaining their shape, and flip-flop [3]. Due to these properties, Pierce beams have potential applications in optical tweezers, imaging systems, etc., thus triggering extensive research by researchers. A growing number of researchers are now investigating the dynamic characteristics of odd Pierce beams [4], toroidal Pierce beams [5], vortex Pierce beams [6], and elliptical Pierce beams [7], which are derived from Pierce beams in free space. Similar to the Airy beam [8], the energy of the Pierce beam is theoretically infinite. However, to produce Pierce beams with restricted energy in experiments while maintaining their properties, one may generate Pierce-Gaussian beams by modulating them with Gaussian beams [9,10,11,12,13]. The beams exhibit a combination of properties derived from both Pierce beams and Gaussian beams. By manipulating the truncation factor, one can modify the field strength of the beams, hence changing the width ratio of the Pierce-Gaussian beams. Furthermore, researchers have also shown interest in the self-focusing characteristics of chirped Pierce pulses and the impact of the initial chirp on the propagation properties of Pierce beams [14,15]. The findings in this study significantly contribute to our understanding of the dynamic characteristics of Pierce beams. Moreover, the new application prospect in the field of optics is introduced.

Researchers have recently undertaken deep research on the propagation characteristics of Pierce beams in various fiber media. Such media include free space [16], Kerr nonlinear media [17,18], strongly non-local nonlinear media [19], multimode fibers [20], and optical lattices with various forms of potential Wells [21,22]. In 2008, Musslimani et al. [23] initially observed optical solitons in PT-symmetric media [24,25]. Later, the researchers analyzed the development of optical solitons in PT-symmetric systems with varying complex refractive indices, such as hyperbolic and Gaussian distributions. In these studies,the soliton properties such as stability, power oscillation and birefringence were investigated [26,27,28,29]. PT-symmetric media are typical of non-uniform, dissipative media with unique optical properties. On the other hand, the Pierce beam is a new type of special beam with properties such as self-focusing and self-healing, which has a wide range of prospects in practical applications. Hence, it is precious from the theory perspective to examine the propagation of Pierce-Gaussian beams in PT-symmetric media. This research contributes to an in-depth understanding of the behavior of optical propagation in PT-symmetric media. It provides potential opportunities for the development of novel devices and

Manuscript received December 14, 2023; revised July 16, 2024.

This work was supported in part by the Natural Science Foundation of Hunan Province under grant numbers 2022JJ50276 and 2023JJ50352, and the Scientific Research Fund of Hunan Provincial Education Department under grant numbers 20B107, 21A0499 and 23B0744.

Zhengchun Zhao is a professor of the College of Information and Electronic Engineering, Hunan City University, Yiyang 413000, China (e-mail: zhaozhengchun@hncu.edu.cn).

Bing Wen is a professor of the College of Information and Electronic Engineering, Hunan City University, Yiyang 413000, China (corresponding author to provide phone: +86-15387409391; e-mail: wenbing@hncu.edu.cn).

Yangbao Deng is a professor of the College of Information and Electronic Engineering, Hunan City University, Yiyang 413000, China (corresponding author to provide phone: +86-15973070033; e-mail: dyb5202008@aliyun.com).

Chunhui Gao is a lecturer of the College of Information and Electronic Engineering, Hunan City University, Yiyang 413000, China (e-mail: gaochunhui@hncu.edu.cn).

Lixiong Li is an assistant professor of the Department of the College of Mechanical and Electrical Engineering, Hunan City University, Yiyang, 413000, China (e-mail: lixiong.li@hncu.edu.cn).

Sheng li is a lecturer of the College of Information and Electronic Engineering, Hunan City University, Yiyang 413000, China (e-mail: lisheng@hncu.edu.cn).

applications in the field of optics.

Previous research has focused on examining the evolutionary characteristics of Gaussian or Airy beams in PT-symmetric media. However, more information is needed on the evolutionary properties of Pierce-Gaussian beams oscillating solitons in PT-symmetric media. To better understand the variation rules of the peak power and center position of the oscillatory soliton generated by the chirped Pierce-Gaussian beams in PT-symmetric medium and to manipulate the oscillatory soliton more efficiently, this paper analyzes in detail the influence of the modulation strength and gain/loss distribution factor of the PT-symmetric medium as well as the chirp coefficients and the truncation coefficients of the chirped Pierce-Gaussian beams on the evolutionary characteristics of the oscillatory soliton. The results of this paper can enrich the soliton species of special beams and provide some theoretical basis for applying PT-symmetric media in all-optical control.

II. Method of Calculation

Under the evening-axis approximation, a Pierce-Gaussian beam propagating in free space follows the following normalized linear Schrödinger equation model:

$$i\frac{\partial\varphi(x,z)}{\partial z}+\frac{1}{2}\frac{\partial^2\varphi(x,z)}{\partial x^2}=0 \tag{1}$$

Where $\varphi(x, z)$ is the dimensionless amplitude of the Pierce-Gaussian beam, $z=Z/Z_0$ denotes the normalized transmission distance in the beam transmission direction, and $x=X/X_0$ denotes the normalized transverse coordinate.

If the Kerr nonlinearity is not taken into account, the beam, when propagated in a Gaussian PT-symmetric optical lattice, can be described by the normalized nonlinear Schrödinger equation [27]:

$$i\frac{\partial\varphi(x,z)}{\partial z}+\frac{1}{2}\frac{\partial^2\varphi(x,z)}{\partial x^2}+V(x)\varphi(x,z)=0 \tag{2}$$

Where $V(x)$ is the potential function and is the complex refractive index of the PT-symmetric medium [25-26]. In this paper, a Gaussian PT-symmetric structure optical lattice is used with the following expression:

$$V(x)=P\left[\exp\left(-x^2\right)+iW_0x\exp\left(-x^2\right)\right] \tag{3}$$

P is the medium's modulation depth, denotes the refractive index distribution strength, and W_0 is the gain/loss distribution strength factor. When the strength of the gain/loss distribution is less than that of the refractive index distribution, i.e., $|W_0|<0$, the eigenvalues of the PT-symmetric system are real. In this paper, we only consider the case of real eigenvalues.

Figure 1(a) illustrates the real and imaginary curves of the Gaussian-type PT-symmetric potential. The real part has even symmetry, whereas the imaginary part demonstrates odd symmetry, satisfying the fundamental requirements of PT symmetry. According to the real part plot, it can be seen that the real part is greater than 0 in the whole transverse region, and at the position of x=0, the real part value is the largest, while away from x=0, the real part value gradually tends to zero. This shows that the refractive index is at its maximum at the center of the PT-symmetric waveguide, while away from the center, the refractive index gradually decreases to equal the basal refractive index. Based on the plot of the imaginary part, the following can be observed: since $W_0 > 0$, the value of the imaginary part is ≤ 0 in the region $x < 0$, while the value of the imaginary part is ≥ 0 in the region $x > 0$, and the absolute value of $W(x)$ reaches its maximum near $x = 0$ (at about x = 0.7). As one moves away from the center position, the value of the imaginary part gradually converges to zero. This indicates that the optical lattice exhibits loss characteristics in the region where $x<0$ and near the center of the waveguide and gain features in the region where $x>0$. And away from the center region, both gain/loss gradually converge to 0.

Upon the propagation of the initial incident beam in free space, the Fourier transform is applied to both sides of Equation (1), resulting in the derivation of the frequency domain equations in the subsequent format:

$$i\frac{\partial\hat{\varphi}(\omega,z)}{\partial z}+\frac{1}{2}\omega^2\hat{\varphi}(\omega,z)=0 \tag{4}$$

Here, the spectrum $\hat{\varphi}(\omega,z)=\int_{\infty}^{-\infty}\varphi(\omega,z)e^{-i\omega x}dx$ is the Fourier transform form of $\varphi(x, z)$, and ω is the inverse space coordinate. In the inverse space, the solution of equation (4) can be easily given [15-16,21]:

$$i\frac{\partial\hat{\varphi}(\omega,z)}{\partial z}+\frac{1}{2}\omega^2\hat{\varphi}(\omega,z)=0 \tag{5}$$

Where $\hat{\varphi}(\omega,0)$ represents the Fourier transform form of the initial incident beam $\varphi(x,0)$. Applying the Fourier transform to both sides of equation (5), the dynamic solution of the beam in free space is obtained as follows:

$$\begin{aligned}\varphi(x,z)&=\frac{1}{2\pi}\int_{-\infty}^{+\infty}\left\{\begin{matrix}\varphi(\omega,0)e^{i\omega x}\times\\ \exp\left(-i\frac{1}{2}\omega^2z\right)\end{matrix}\right\}d\omega\\&=\frac{(1-i)}{2\sqrt{\pi z}}\int_{-\infty}^{\infty}\left\{\begin{matrix}\varphi(\xi,0)\times\\ \exp\left(\frac{i(x-\xi)^2}{2z}\right)\end{matrix}\right\}d\xi\end{aligned} \tag{6}$$

Similarly, the solution for the dynamics of the incident beam in a PT-symmetric medium can be found as a Fourier transform of both sides of its transmission equation (2):

$$\left\{\begin{matrix}i\frac{\partial\hat{\varphi}(\omega,z)}{\partial z}-\frac{1}{2}\omega^2\hat{\varphi}(\omega,z)+\\ \frac{1}{2\pi}\hat{V}(\omega)*\hat{\varphi}(\omega,z)\end{matrix}\right\}=0 \tag{7}$$

where $\hat{V}(\omega)$ is the Fourier transform of Eq. (3) with the following expression:

$$V(\omega)=\frac{1}{2}P\sqrt{\pi}\exp\left(\frac{-\omega^2}{4}\right)(W_0\omega+2) \tag{8}$$

Solving equation (7) gives:

$$\hat{\varphi}(\omega,z)=\hat{\varphi}(\omega,0)\exp\left(-i\frac{1}{2}\omega^2z+iz\upsilon\right) \tag{9}$$

Where υ is the convolution of the spectrum of the initial incident beam $\varphi(x,0)$ and the spectrum of the potential function $V(x)$ with the following expression:

$$\begin{aligned}\upsilon&=\frac{1}{2\pi}V(\omega)*\varphi(\omega,0)\\&=\frac{1}{2\pi}\int_{-\infty}^{+\infty}V(\omega-\eta)\varphi(\eta,0)d\eta\end{aligned} \tag{10}$$

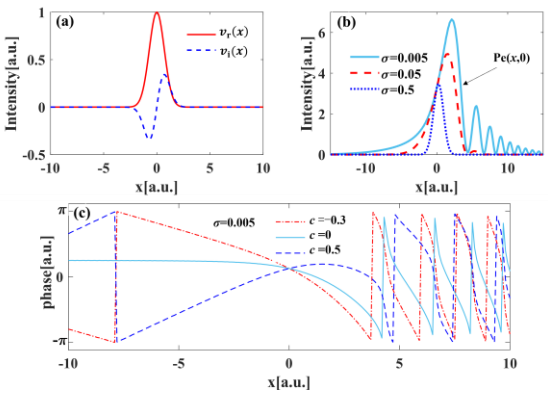

Fig. 1 (a) Plot of complex refractive index distribution for Gaussian-type PT-symmetric medium; (b) Distribution of intensity at c = -0.3 for various truncation factors σ; (c) Plot of phase distribution for σ = 0.005 and different chirp factors c.

A further Fourier transform of both sides of Eq. (9) yields a solution for the dynamics of the incident beam in a Gaussian-type PT-symmetric medium:

$$\varphi(x,z)=\frac{1}{2\pi}\int_{-\infty}^{+\infty}\left\{\begin{matrix}\varphi(\omega,0)e^{i\omega x}\times\\ \exp\left(-i\frac{1}{2}\omega^2 z+iz\upsilon\right)\end{matrix}\right\}d\omega \qquad (11)$$

The initial input beam used is a chirped Pierce-Gaussian beam, which has the following form:

$$\varphi(x,0)=Pe(x,0)\exp\left(-\sigma x^2\right)\exp(icx) \qquad (12)$$

Where σ is the truncation factor, c is the initial chirp, and $Pe(x,0)$ is the Pierce function. The expression for $Pe(x,0)$ is given below:

$$Pe(\mathrm{x},0)=\int_{-\infty}^{+\infty}ds\exp\left[\mathrm{i}\left(as^4+s^2\mathrm{x}/b\right)\right] \qquad (13)$$

Where a is the coefficient of the integral term and b is the scaling factor. By Substituting the spectrum of the incident beam represented by Equation (12) into Equation (11), we can obtain the light intensity distribution function when propagating in Gaussian-type PT symmetric medium. The plot of the light intensity distribution corresponding to different truncation factors σ [Fig. 1 (b)] shows that the chirped Pierce-Gaussian beam exhibits an asymmetric trailing oscillatory structure, with the highest energy of the main peak, many paraboloids on the right side, which forms a long trailing tail, and the power of the paraboloids decreases gradually. The truncation factor σ can control the peaks of the main and side peaks. When σ is 0.005, the chirped Pierce-Gaussian beam shows a clear multi-peak structure. As the truncation factor σ gradually increases, the waveform gradually approaches a Gaussian function. When σ is 0.005, the chirped Pierce-Gaussian beam shows a clear multi-peak structure. Through the phase distribution plots of chirped Pierce-Gaussian beams corresponding to different chirp coefficients c [Fig. 1 (c)], it is evident that the phase of each varies from -π to π continuously. When the chirp is positive, the phase change is ahead, while when the chirp is negative, the phase change is lagging.

III. Results and Discussion

This work investigates the characteristics of chirped Pierce-Gaussian beams propagated in PT-symmetric media in free space. Because of its gain-dissipation property, similar to that of natural media, it is of great practical importance to study beam transport in PT-symmetric media. Below, we shall explore the dynamic characteristics of chirped Pierce-Gaussian in free space and Gaussian-type PT-symmetric media, respectively.

A. Self-focusing behavior of chirped Pierce-Gaussian beams in free space

Figure 2 illustrates the evolutionary properties of the incident beam in free space for different truncation factors σ and chirp coefficients c. Observably, each part of the Pierce beam is experiencing acceleration in a sideways direction. Moreover, the acceleration becomes more evident as the distance from the central section increases. Consequently, this causes the main section and the side sections to meet together at z = 2 [Fig. 2 (a1)-(c1)]. After passing this point, the acceleration changes direction and becomes negative along the x-axis. The beam starts to slow down in a sideways direction, with the outer part of the para lobe decelerating more rapidly. This causes the main and para to separate and the intensity distribution to invert. Eventually, a focus-flip evolutionary pattern is formed. The truncation factor determines a degree of freedom of the waveform of the chirped Pierce-Gaussian beam. When the truncation factor increases, the side lobe of the chirped Pierce-Gaussian beam diminishes and approaches a Gaussian beam. At this juncture, the self-focusing characteristic ceases to exist when transmitted via free space [Fig. 2 (a3)-(c3)]. Moreover, altering the chirp coefficient c leads to a modification in the trajectory of the beam's propagation. For positive values of c, the chirped Pierce-Gaussian beam turns towards the right. Conversely, for negative values of c, the chirped Pierce-Gaussian beam eventually counteracts its initial leftward redirection and is redirected towards the right, owing to the rightward deflection caused by the positive chirp. The phase evolution of the chirped Pierce-Gaussian beam with different initial chirps shows that the chirps lead to phase perturbations in the optical field. This phase perturbation can lead to changes in the propagation characteristics of the beam. When the value of c is greater than 0, the phase of the left side of the center beam during the early stage of beam propagation is positive, leading to a significant overrun of the main flap on the left side [Figure 2 (c4)]. After focusing of the beam occurs, the phase on the right side of the center beam is less than 0, resulting in a significant hysteresis on the right side of the para lobe. When c<0, the phase on the left side of the center beam during the initial stage of beam transmission is less than 0, causing the main lobe on the left side to exhibit significant lag. After the beam focuses, the phase on the right side of the center beam is greater than 0, causing the side lobe on the right side to exhibit significant lead. Therefore, a negative initial chirp causes the chirped Pierce-Gaussian beam to significantly deflect clockwise, while a positive initial chirp produces the opposite effect [Figure 2 (a4)]. Therefore, a positive initial chirp causes the chirped Pierce-Gaussian beam to significantly rotate clockwise around the focal point, while a negative initial chirp causes the beam to significantly rotate counterclockwise around the focal point.

Figure 3(a) shows the peak intensity at the focal point of the chirped Pierce-Gaussian beam and the variation of the

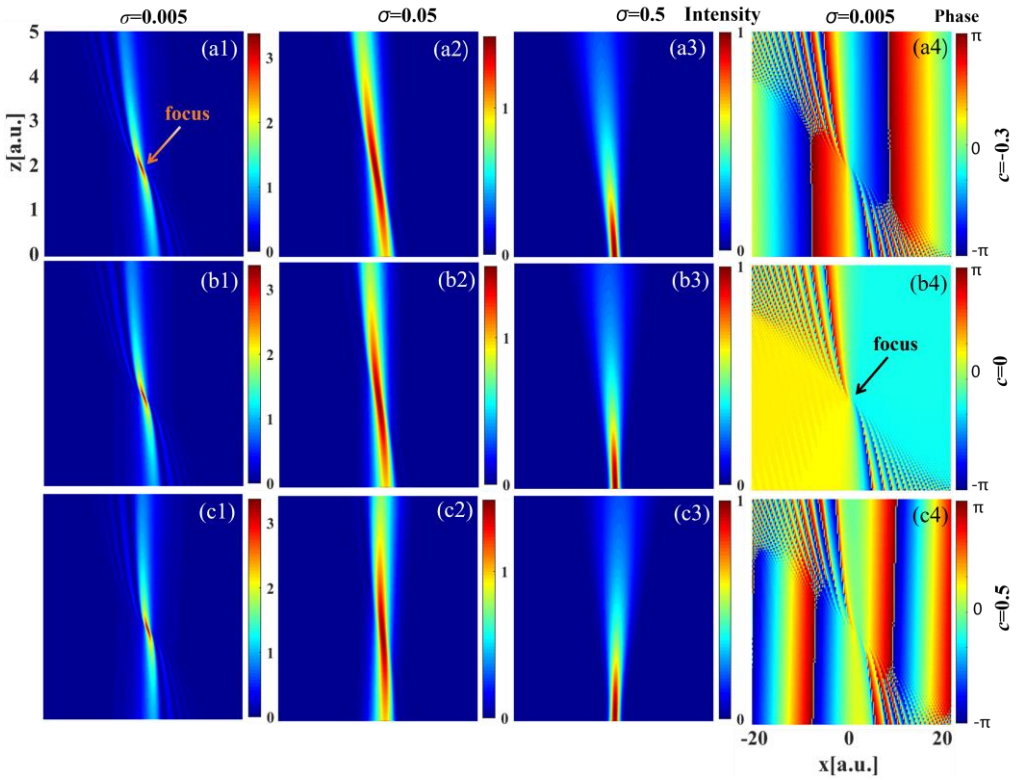

Fig. 2 Intensity evolution plots at different truncation factors: (a1)- (a3) c =-0.3, (b1)- (b3) c=0, (c1)- (c3) c=0.5; and phase evolution plots at different chirp coefficients for (a4)- (c4) σ=0.005.

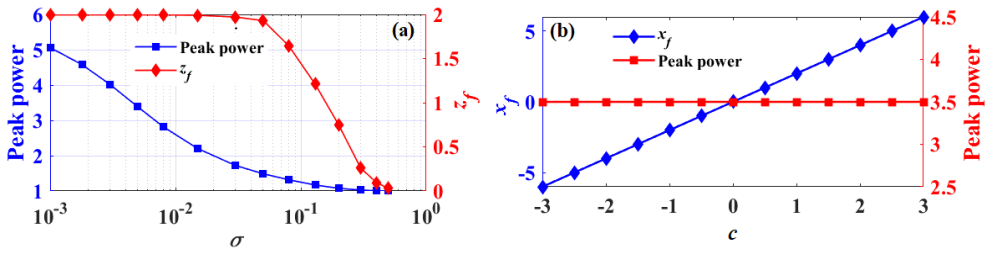

Fig. 3 (a) Plot of the peak intensity of the focal point and the variation of the vertical coordinate with the truncation factor; (b) Plot of the peak intensity of the focal point and the variation of the horizontal coordinate with the chirp.

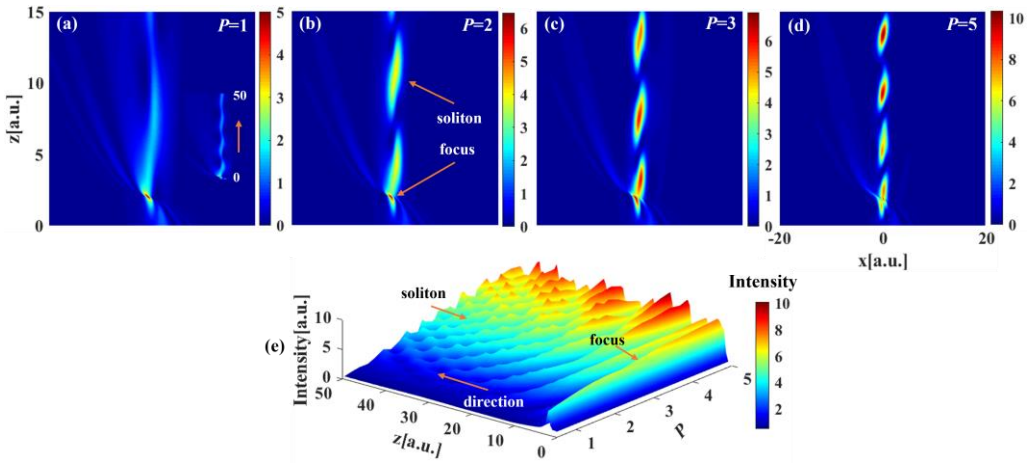

Fig. 4 (a)-(d) Spatial evolution of Pierce-Gaussian beams in PT-symmetric media with different modulation depths; (e) Plot of the optical field intensity as a function of propagation distance and modulation depth.

vertical coordinate z_f with σ. As the truncation factor σ increases, the deceleration of the peak strength of the focus decreases. When $\sigma < 0.05$, the vertical coordinate of the focal point $z_f = 2$ remains essentially constant. And z_f decreases rapidly to 0 when $\sigma > 0.05$, which is due to the fact that the chirped Pierce-Gaussian beam converges to a Gaussian beam at this point, and the side lobe almost disappears, and its self-focusing behavior diminishes rapidly. Fig. 3(b) shows a plot of the transverse coordinates of the focal point of the chirped Pierce-Gaussian beam versus the peak intensity

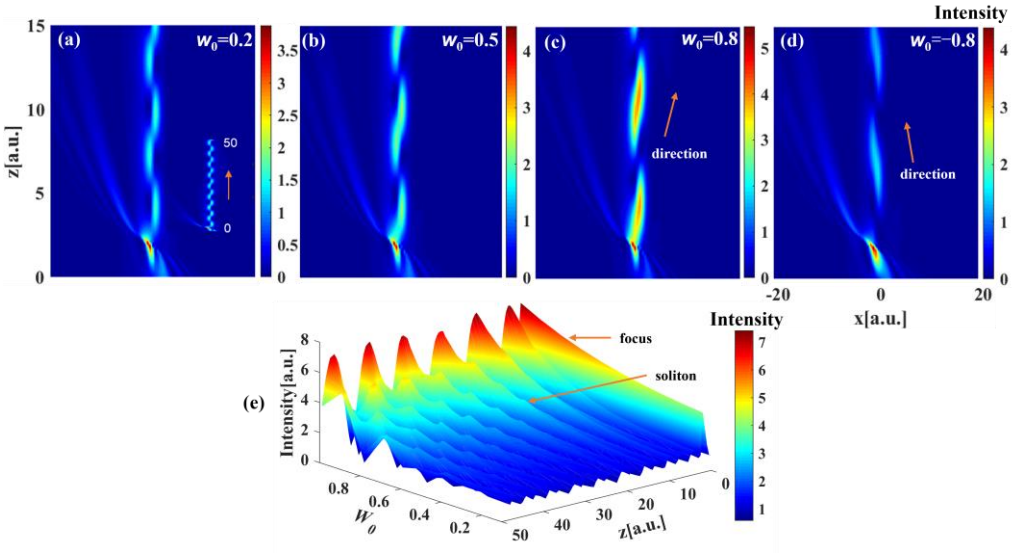

Fig. 5 (a)-(d) Spatial evolution of chirped Pierce-Gaussian beams in PT-symmetric media with different gain/loss coefficients; (e) Plot of the optical field intensity as a function of propagation distance and gain/loss coefficient.

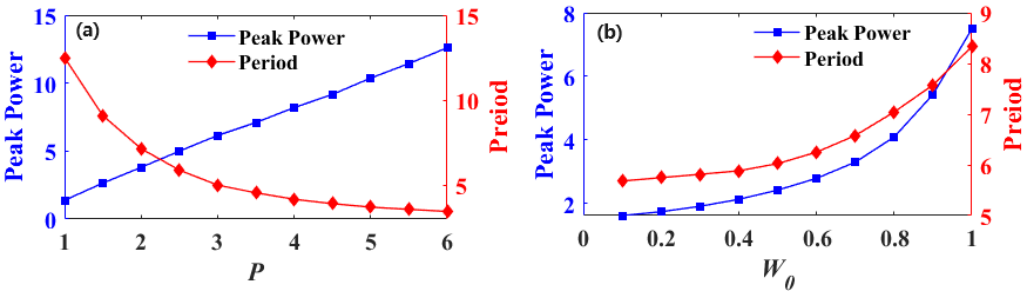

Fig. 6 (a) Plot of the maximum intensity and oscillation period of the shedding soliton as a function of modulation depth; (b) Plot of the maximum intensity and oscillation period of the soliton as a function of gain/loss coefficient.

variation with the initial chirp c. It is evident that x_f exhibits a linear relationship with c, where x_f is negative for $c < 0$ and positive for $c > 0$. The initial value of c does not impact the maximum intensity of the focus. The above features show that the truncation coefficient of the chirped Pierce-Gaussian beam controls the peak intensity of the focal point and the position of the focal point in the direction of propagation during free-space propagation, while the initial chirp controls the direction of deflection of the beam and the transverse position of the focal point.

B. Shedding of chirped Pierce-Gaussian oscillatory solitons in Gaussian-type PT-symmetric media

Figure 4 shows the propagation of the incident beam in a PT-symmetric medium with a Gaussian profile, where the modulation depths P vary. The parameters used are $\sigma = 0.005$, $c = -0.3$, and $W_0 = 0.8$. Due to the self-focusing property of the chirped Pierce-Gaussian beam, the chirped Pierce-Gaussian beam undergoes a compression phase in the initial stage, leading to an increase in the peak power and an increase in the nonlinear modulation effect. Finally, a soliton is shed at the focus of the chirped Pierce-Gaussian beam at its main peak. The soliton eventually stabilizes into an oscillating soliton with a periodically varying peak power and width during transmission, and at this point, the soliton contains most of the beam's energy. The main peak loses a significant amount of its energy by emitting of a soliton, while the remaining energy gradually returns to the Pierce shape as a result of the inherent self-recovery characteristics of the chirped Pierce-Gaussian beam [Fig.4(a)]. The modulation strength gradually increases, i.e., the refractive index in the PT-symmetric medium also gradually increases, then its ability to bind light is also gradually increasing [Figs. 4(b)-(d)], increasing the peak power of the oscillatory soliton [Fig.4(e)], and the period becomes smaller. The above explanation demonstrates that the modulation strength P can govern the maximum intensity and the period of oscillation of the Pierce-Gaussian beam shedding soliton

Fig. 5 shows the evolution of the incident beam in Gaussian-type PT-symmetric media with different W_0 for $\sigma = 0.005$, $c = -0.3$ and $P = 2$. The strength of the gain/loss distribution W_0 causes the shedding solitons to appear in different directions and magnitudes of the lateral energy flow during transmission. When the value of W_0 is small [Fig. 5(a)], the shedding soliton has less lateral energy flow during transport. As the value of W_0 gradually increases, the lateral flow of soliton energy also gradually increases [Fig. 5(b)-(c)]. And when $W_0<0$, the direction of transmission is opposite to that at the strength of the gain/loss distribution [Fig. 5(d)]. It is because when $W_0<0$, the $x<0$ region presents a loss, so the soliton flows energy to the left first to the loss region during transmission. However, due to the optical lattice center refractive index of light binding, the shedding soliton again to the right folded back to the center region and flowed to the gain region so that the cycle continued to form a wave-shaped beam. Hence, it is evident that the soliton deflection direction and deflection size can be manipulated by the positive or

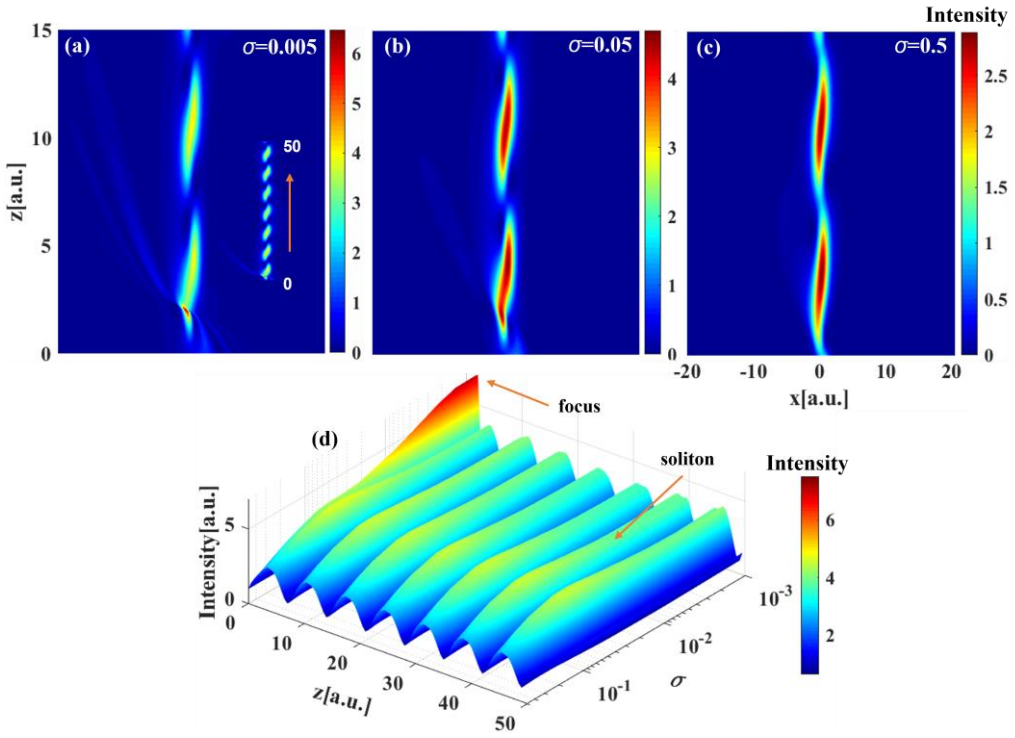

Fig. 7 (a)-(c) Spatial evolution of Pierce-Gaussian beams in PT-symmetric medium for different cutoff coefficients; (d) Variation of optical field intensity with propagation distance and cutoff coefficient.

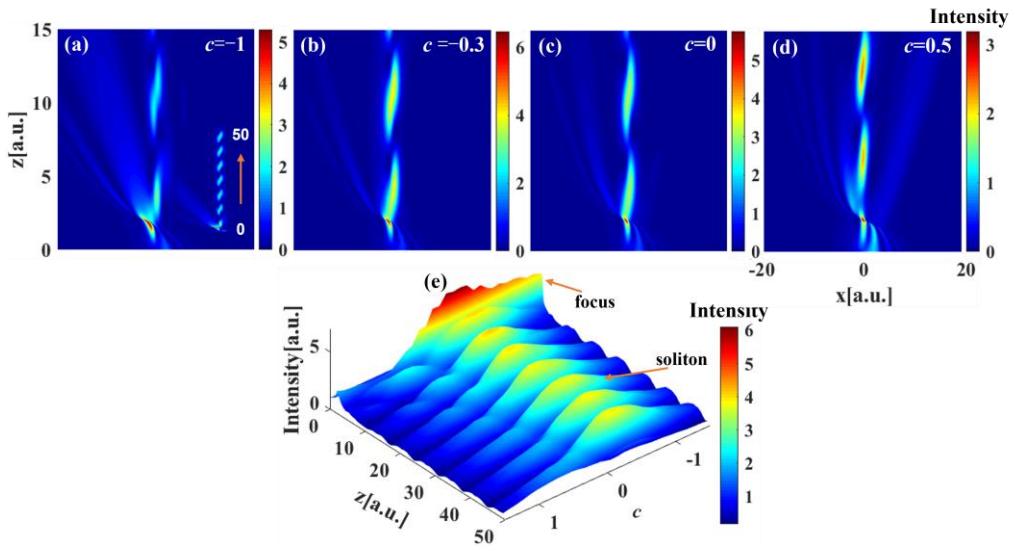

Fig. 8 (a)-(d) Spatial evolution of Pierce-Gaussian beams in PT-symmetric medium with different chirps; (e) Plot of optical field intensity versus propagation distance and chirp.

negative gain/loss intensity of the complex refractive index. The larger the absolute value of the gain/loss distribution strength W_0, the larger the peak power of the oscillatory soliton and the larger the period [Fig. 5 (e)].

Fig. 6(a) shows a plot of the peak intensity and oscillation period of the soliton versus P. The peak intensity of the soliton increases approximately linearly with P, and the period of oscillation decelerates and decreases with P. This indicates that the modulation depth of the PT-symmetric medium is proportional to the magnitude of the refractive index at the center of the waveguide. The increase in the refractive index of the waveguide causes the energy of the incident light's side lobes to converge to the main lobes more quickly, forming exfoliated solitons. Figure 6(b) shows a quantitative plot of the soliton's peak intensity and oscillation period versus W_0. This demonstrates that as W_0 increases, both the soliton's peak intensity and oscillation period experience acceleration. When W_0 is small, the lateral flow of soliton energy is small; when W_0 increases, the lateral flow of soliton energy increases.

The truncation factor σ is an additional degree of freedom of the chirped Pierce-Gaussian beam, which controls the distribution of the intensity of the light field in the main and side flaps of the beam. The evolution of chirped Pierce-Gaussian beams in Gaussian-type PT-symmetric media with different values of the truncation factor σ is given

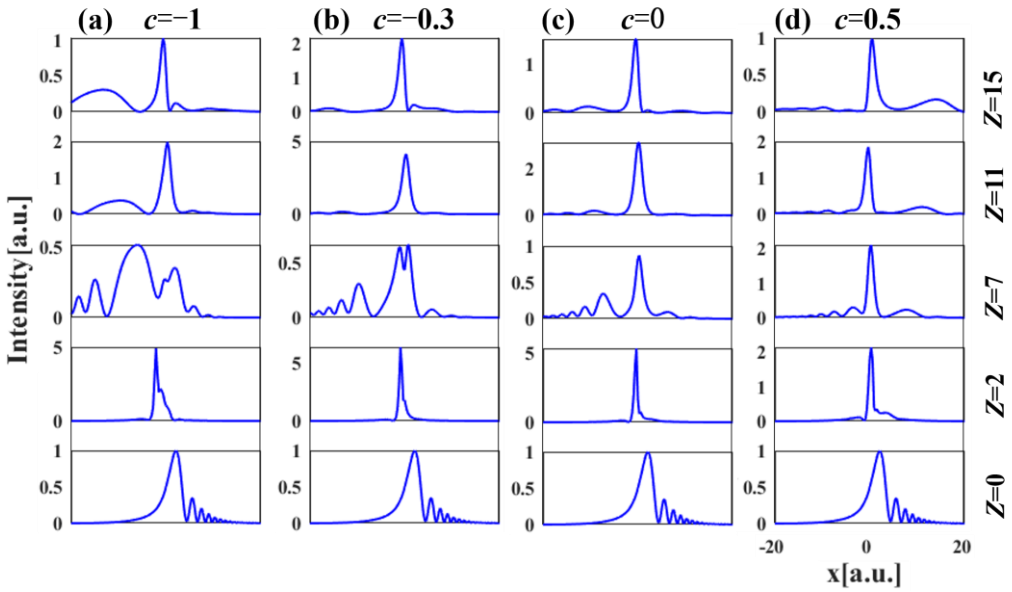

Fig. 9 (a)-(d) Intensity profiles of differently chirped Pierce-Gaussian beams at different propagation distances.

in Fig. 7 for $P = 2$, $W_0 = 0.8$ and $c = -0.3$. When σ is very small, the intensity of the main peak of the chirped Pierce-Gaussian beam is large, and the peak power of the exfoliated soliton formed is also large [Fig. 7(a)]. When the truncation factor σ increases, the peak intensity of the focus gradually decreases, and the para lobe gradually weakens until it disappears, but the period of oscillation of the soliton does not change [Figs. 7(b), (c)]. Figure 7(d) gives the variation of light intensity of the chirped Pierce-Gaussian beam for transmission distances from 0 to 50 and truncation factors from 0.001 to 1. It can be seen that the peak intensity of the soliton increases slowly as the truncation factor σ increases with an exponential rate of change for $\sigma < 0.1$, and the smaller σ is, the more stable the peak intensity of the soliton is, whereas the peak of the focus decreases with the increase of σ. When $0.1 < \sigma < 1$, the peak intensity of the soliton decreases rapidly with increasing σ. This is because the Pierce-Gaussian beam at $\sigma > 0.1$ has evolved into a Gaussian beam. The above phenomenon indicates that the truncation factor controls the peak intensity of the shed soliton when transmitted in PT-symmetric media.

The evolution of the Pierce-Gaussian beam in a Gaussian PT-symmetric medium for different chirp coefficients c is given in Fig. 8 for $P = 2$, $W_0 = 0.8$, and $\sigma = 0.005$. It can be seen that the value of c affects both the peak intensity of the soliton and the peak intensity of the focus but does not affect the soliton's oscillation period. When $c<0$, the remaining para lobe after soliton shedding continues to be deflected in the counterclockwise direction, and when $c>0$, the para lobe is deflected in the clockwise direction [Figs. 8(a)-(d)], which is consistent with the deflection of the beam as it is propagated in free space. Figure 8(e) gives the variation of light intensity of the chirped Pierce-Gaussian beam for transmission distances from 0 to 50 and chirp factors from -1.5 to 1.5. When $c = -0.3$, the soliton peak intensity reaches a maximum, and when $|c|$ increases, the peak intensity of the soliton is gradually weakened. The above shows that chirped Pierce-Gaussian beams, when transmitted in Gaussian-type PT-symmetric media, can control the magnitude of the peak intensity of the detached soliton and the direction of deflection of the side lobe.

Figures 9(a)-(d) show the waveform evolution of the chirped Pierce-Gaussian beam at different transmission distances over two cycles, respectively. The chirped Pierce-Gaussian beam is focused at a transmission distance of 2 when the peak intensity reaches a maximum, at which point exfoliated solitons form. When $c > 0$, the center of the shedding soliton is located at the positive semiaxis of the x-axis [Fig. 8(d)]. And when $c<0$, the center position of the shedding soliton is in the left half-axis of the x-axis [Fig. 8(a)-(d)], and the smaller c is, the larger the shift of the center position of the shedding soliton is.

IV. Conclusion

The investigation analyses the propagation laws of chirped Pierce-Gaussian beams in free space and Gaussian-type PT-symmetric media using the nonlinear Schrödinger equation as a theoretical model. The results show that the self-focusing intensity of the chirped Pierce-Gaussian beam gradually increases as the value of the truncation factor σ decreases when propagated in free space. When $\sigma < 0.05$, the beam still maintains the self-focusing property and the focal position is located at $z = 2$. However, when $\sigma > 0.05$, the beam converges to a Gaussian beam, and the self-focusing property disappears. Furthermore, altering the value of c causes the beam's propagation direction to deviate. Specifically, when c is negative, the deflection direction is anticlockwise; when c is positive, the deflection direction is clockwise. Additionally, the deflection angle rises as the absolute value of c grows. When propagated in a PT-symmetric medium with a Gaussian profile, the Pierce-Gaussian beam exhibits oscillatory soliton propagation at the focal point. As the modulation strength P increases, the peak intensity of the soliton increases while the period decreases. As the gain/loss coefficient W_0 increases, both the peak intensity and period of the soliton increase. When the truncation factor $\sigma < 0.1$, the peak intensity of the soliton increases slowly as the truncation factor σ increases with an exponential rate of change, and when $0.1 < \sigma < 1$, the peak intensity of the soliton decreases rapidly as the truncation factor σ increases. Meanwhile, the

chirp coefficient c can modulate the peak intensity of the soliton as well as the deflection direction of the side lobe. When $c<0$, the shedding soliton is deflected in a counterclockwise direction, and when $c>0$, it is deflected in a clockwise direction. The analysis focuses on the waveform evolution of a chirped Pierce-Gauss beam in a PT-symmetric medium. The study examines the beam's behaviour at various propagation distances across two cycles and investigates how chirping affects beam deflection. The results of this study provide a theoretical basis for studying the transport dynamics of special beams in complex media and the soliton transport properties.

REFERENCES

[1] Pearcey T, "The structure of an electromagnetic field in the neighbourhood of a cusp of a caustic," *Phil Mag Sci*, vol.37, pp 311-317, 1946.

[2] James D R, Jari L, Areti M, et al., "Auto-focusing and self-healing of Pearcey beams," *Opt. Express*, vol.20, no.17, pp 18955-18966, 2012.

[3] Deng D M, Chen C D, Zhao X, et al., "Virtual source of a Pearcey beam," *Opt. Lett.*, vol.39, no.9, pp 2703-2706, 2014.

[4] Liu Y J, Xu C J, Lin Z J, et al., "Auto-focusing and self-healing of symmetric odd-Pearcey Gauss beams," *Opt. Lett.*, 2020, vol.45, no.11, pp 2957–2960, 2020.

[5] Chen X Y, Deng D M, Zhuang J L, et al., "Focusing properties of circle Pearcey beams," *Opt. Lett.*, vol.43, no.15, pp 3626–3629, 2018.

[6] Wu Y, He S L, Wu J H, et al. "Autofocusing Pearcey-like vortex beam along a parabolic trajectory," *Chaos Solitons Fractals*, vol.145, pp 110781, 2021.

[7] Jiang J J, Mo Z W, Xu D L, et al. "Elliptical Pearcey beam," *Opt. Commun.*, 2022, 504:127475.

[8] Siviloglou G A, Broky J, Dogariu A. "Ballistic dynamics of Airy beams," *Opt. Lett.*, vol.33, no.3, pp 207–209, 2008.

[9] Chen X Y, Deng D M, Zhuang J L, et al. "Nonparaxial propagation of abruptly autofocusing circular Pearcey Gaussian beams," *Appl. Opt.*, vol.7, no.28, pp 8418–8423, 2018.

[10] Zhou X Y, Pang Z H, Zhao D M. "Partially coherent Pearcey–Gauss beams," *Opt. Lett.*, vol.5, no.9, pp 5496–5499 2018.

[11] Sun C, Deng D M, Yang X B. "Propagation dynamics of autofocusing circle Pearcey Gaussian vortex beams in a harmonic potential," *Opt. Express*, vol.28, no.1, pp 325-331, 2020.

[12] Mo Z W,Wu Y, Lin Z J, et al. "Propagation dynamics of the odd-Pearcey Gaussian beam in a parabolic potential," *Appl. Opt.*, vol.60, no.23, pp 6730–6735, 2021.

[13] Fang M Y, Liao X, Zhao J J, et al."Paraxial propagation properties of radially polarized odd-Pearcey Gaussian beams in free space," *Ann. Phys.-Berlin*, vol.533, no.6, pp 2100055, 2021.

[14] Chen X Y, Deng D M, Wang G H, et al. "Abruptly autofocused and rotated circular chirp Pearcey Gaussian vortex beams," *Opt. Lett.*, vol.44, no.4, pp 955-958.

[15] Zang F, Liu L F, Deng F S, et al. "Dual-focusing behavior of a one-dimensional quadratically chirped Pearcey-Gaussian beam," *Opt. Express*, vol.29, no.16, pp 26048-26057, 2021.

[16] Zhan K Y, Kang X Y, Dou L C, et al. "Scaling quasi-self-imaging effect based on the one- dimensional Pearcey beam," *J. Opt. Soc. Am. B*, vol.39, no.3, pp 751-755, 2022.

[17] Li Y Q, Peng Y Q, Hong W Y. "Propagation of the Pearcey pulse with a linear chirp," *Results Phys.*, vol.16, pp 102932, 2020.

[18] Zhang L P, Chen X Y, Deng D M, et al. "Dynamics of breathers-like circular Pearcey Gaussian waves in a Kerr medium," *Opt. Express*, vol.27, no.13, pp 17482-17492.

[19] Huang Z C, He J J, Xu D L, et al. "Propagation of Pearcey Gaussian beams in a strongly nonlocal nonlinear medium," *Appl. Opt.*, vol.60, no.32, pp 10168, 2021.

[20] Xu C J, Wu J H, Wu Y, et al. "Propagation of the Pearcey Gaussian beams in a medium with a parabolic refractive index," *Opt. Commun.*, vol.464, pp 125478, 2020.

[21] Gao R, Ren S M, Guo T, et al. "Propagation dynamics of chirped Pearcey-Gaussian beam in fractional Schrödinger equation under Gaussian potential," *Optik*, vol.254, pp 168661, 2022.

[22] M. Y. Hamza, Sumaira Saeed, N. Sarwar, and S. Yang, "Investigations for the Evolution Behavior of Cos-Gauss Pulse in Dispersion Dominant Regime of Single Mode Optical Fiber," *Engineering Letters*, vol. 22, no. 2, pp83-86, 2014.

[23] El-Ganainy R, Makris K G, Christodoulides D N, et al. "Theory of coupled optical PT-symmetric structures," *Opt. Lett.*, vol.32, no.17, pp 2632-2634, 2007.

[24] Musslimani Z H, Makris K G, El-Ganainy R, et al. "Optical solitions in PT periodic porentials," *Phys. Rev. Lett.*, vol.100, no.3, pp 030402, 2008.

[25] Chen R H, Hong W Y. "Dynamics of Airy beams in parity–time symmetric optical lattices," *Chin. Phys. B*, vol.28, no.5, pp 054202, 2019.

[26] Deng Y B, Wen B, Chen L Z, et al. "Propagation properties of cosh-Airy beams in an inhomogeneous medium with Gaussian PT-symmetric potentials," *Open Phys.*, vol.20, pp 1031-1040, 2022.

[27] Yao G, Chew K, Wu Y, et al. "Propagation dynamics of vector vortex beams in a trongly nonlocal nonlinear medium with parity-time-symmetric potentials," *J. Optics*, vol.24, no.3, pp 035606, 2022.

[28] Huang C F, Zeng J L. "Solitons stabilization in PT symmetric potentials through modulation the shape of imaginary component," *Opt. Laser Technol.*, vol.35, no.6, pp 104-110, 2017.

[29] Qiu Y L, Malomed B A, Mihalache D, et al. "Soliton dynamics in a fractional complex Ginzburg-Landau model," *Chaos Solitons Fractals*, vol.131, pp 108471, 2020.